Nanorod Mobility within Entangled Wormlike Micelle Solutions

Jonghun Lee, ¹ Aline Grein-Iankovski, ² Suresh Narayanan, ¹ and Robert L. Leheny ³

¹X-ray Science Division, Argonne National Laboratory, Argonne, Illinois 60439, USA

²Department of Chemistry, Federal University of Parana, Curitiba, PR, Brazil

³Department of Physics & Astronomy, Johns Hopkins University, Baltimore, Maryland 21218, USA

Abstract

In the semi-dilute regime, wormlike micelles form an isotropic entangled microstructure that is similar to that of an entangled polymer solution with a characteristic, nanometer-scale entanglement mesh size. We report a combined x-ray photon correlation spectroscopy (XPCS) and rheology study to investigate the translational dynamics of gold nanorods in semi-dilute solutions of entangled wormlike micelles formed by the surfactant cetylpyridinium chloride (CPyCl) and the counter-ion sodium salicylate (NaSal). The CPyCl concentration is varied to tune the entanglement mesh size over a range that spans from approximately equal to the nanorod diameter to larger than the nanorod length. The NaSal concentration is varied along with the CPyCl concentration so that the solutions have the maximum viscosity for given CPyCl concentration. On short time scales the nanorods are localized on a length scale matching that expected from the high-frequency elastic modulus of the solutions as long as the mesh size is smaller than the rod length. On longer time scales, the nanorods undergo free diffusion. At the highest CPyCl concentrations, the nanorod diffusivity approaches the value expected based on the macroscopic viscosity of the solutions, but it increases with decreasing CPyCl concentration more rapidly than expected from the macroscopic viscosity. A recent model by Cai et al. [Cai, L.-H.; Panyukov, S.; Rubinstein, M. Macromolecules 2015, 48, 847-862.] for nanoparticle "hopping" diffusion in entangled polymer solutions accounts quantitatively for this enhanced diffusivity.

I. Introduction

The mobility of nanoparticles within viscoelastic complex fluids impacts a wide range of technologies. For example, in the design and fabrication of nanocomposites, control over the dispersion and partitioning of nanoparticles in polymer melts is crucial for achieving desired material performance.¹⁻⁴ Also, in advanced approaches to drug delivery, the efficacy of nanoparticles as carriers of medicinal cargo relies on their ability to diffuse through biological gels. 5, 6 Nanoparticle dynamics in complex fluids also raises scientific questions that go to the heart of the relationship between the hierarchical microscopic properties of the fluids and their macroscopic rheological response. The significance of these issues has motivated numerous recent experimental, 7-26 theoretical, 27-34 and simulation studies 35-39 to investigate nanoparticle dynamics within polymer melts and solutions and related materials. Polymers are characterized by several microscopic length scales, including the correlation length and radius of gyration, and in the case of entangled solutions, the tube diameter and entanglement mesh size. When nanoparticles are sufficiently large compared to these intrinsic scales, their mobility reflects the solution's macroscopic viscoelasticity, and under appropriate conditions the particle mean squared displacement $\langle \Delta r^2(t) \rangle$ is related to the creep compliance J(t) of through a generalized Stokes-Einstein relation, 40, 41

$$J(t) = \zeta < \Delta r^2(t) > /6k_B T \tag{1}$$

where ζ is the particle's geometric drag coefficient. However, when the size of the nanoparticles approaches the solution's intrinsic microscopic length scales, this correspondence breaks down, as numerous recent studies have illustrated. For example, nanoparticles in entangled polymers can display mobilities that are orders of magnitude larger than those expected from macroscopic rheology when their size is near or below the entanglement mesh size. Further, in both entangled

and unentangled solutions, nanoparticles can exhibit a regime of anomalous, subdiffusive motion over short distances that reverts to simple diffusion only on scales large compared to the relevant polymer microstructure. 10, 12, 35

In order to obtain an expanded perspective on the relationship between complex-fluid microstructure and nanoparticle mobility, we have conducted experiments employing x-ray photon correlation spectroscopy (XPCS) to interrogate the nanoscale dynamics of rod-shaped nanoparticles within entangled wormlike micelle solutions. Wormlike micelles (WLM) are long, thin, cylindrical aggregates of surfactant molecules that self assemble in aqueous solution under appropriate conditions. Due to the morphology of the assemblies, WLM solutions exhibit structure and rheology similar to polymer solutions, and at sufficient concentration the micelles can entangle, giving the solutions significant viscoelasticity. However, because they are supramolecular assemblies, WLMs grow, break, and reform at rates set by equilibrium thermodynamics, making them "living" polymers and leading to characteristic features in the rheology of the solutions. For instance, over a broad range of conditions, the linear response of WLM solutions approximates that of a Maxwell liquid with a single stress relaxation time, and this behavior is understood to be a consequence of a coupling of micelle reptation to scission and recombination events.⁴² Such distinctive features make WLM solutions an interesting point of comparison with polymer solutions for considering nanoparticle mobility, where the deviations from macroscopic expectations can depend on structural dynamics at the nanoscale.

XPCS provides a unique opportunity to probe nanoparticle mobility over distances spanning the characteristic lengths in nanostructured complex fluids.^{43, 44} Like dynamic light scattering, XPCS tracks temporal fluctuations in coherent scattering intensity; however, the much shorter wavelengths of x-rays compared with visible light enables the technique to access

dynamics on smaller length scales. Here, we employed XPCS to study the Brownian motion of gold nanorods in entangled WLM solutions formed by the surfactant cetylpyridinium chloride (CPyCl) with the counter-ion sodium salicylate (NaSal). CPyCl/NaSal is a model WLM system whose macroscopic rheology has been well characterized.⁴² By varying the surfactant concentration, we tuned the entanglement mesh size from values smaller than the nanorod diameter to values larger than the nanorod length. This investigation of nanorod dynamics complements studies of nanosphere mobility in entangled polymer solutions. As previous work exploring nanorod dynamics in entangled polymers has illustrated,^{11, 14, 27} the rods' anisotropic shape provides an insightful perspective on the relationship between particle dimension and solution microstructure in dictating mobility.

As described below, we find that the nanorods remain elastically coupled to the WLM entangled network on short times provided the length L of the rods is larger than the entanglement mesh size \mathcal{E} . However, the diffusivity of the rods on longer time exceeds that expected from the solutions' macroscopic viscosity over a range of mesh sizes extending to sizes as small as $\mathcal{E} \approx L/4$. A recent model of nanoparticle mobility in entangled polymer solutions introduced by Cai *et al.*²⁹ that considers a hopping mechanism that acts in parallel with entanglement relaxation to promote particle diffusion in this size regime accounts accurately for the enhanced diffusivity of the nanorods.

II. Materials and Methods

A. Nanorod Synthesis

Gold nanorods were synthesized using seed-mediated growth in solutions of cetyltrimethylammonium bromide (CTAB; TCI America) following procedures reported by Ye

et al.⁴⁵ The nanorods had radius $R = 7.7 \pm 0.8$ nm and length $L = 47.0 \pm 4.4$ nm, as determined by transmission electron microscopy (TEM). (See Figure S1 in the Supporting Information for an example TEM image.) As synthesized, the nanorods were stabilized by excess CTAB that coats the particle surfaces. When mixed into CPyCl/NaSal solutions, these nanorods aggregated, likely because CTAB loses affinity to the gold surfaces and forms micelles in the presence of the salicylate ions. To avoid this problem, the surfaces of the nanorods were functionalized with methoxy polyethyleneglycol thiol (mPEG-SH; Creative PEGWorks) with molecular weight of 2000 g/mol prior to their introduction into the CPyCl/NaSal solutions. The as-synthesized nanorods were centrifuged at 8500 rpm for 25 min twice to remove excess CTAB and then were mixed with 2 mM mPEG-SH aqueous solution for 24 hours. Any remaining CTAB and unreacted mPEG-SH were then removed by multiple centrifugations.

B. WLM Solution fabrication

Desired quantities of CPyCl (Alfa Aesar) and NaSal (Alfa Aesar) were added to dilute stock solutions of the mPEG-functionalized nanorods to prepare WLM solutions with varying concentration. Small angle x-ray scattering (SAXS) profiles from the solutions followed closely the form factor of isolated rods, with no signs of aggregation. (See Figures S2 and S3 in the Supporting Information for example SAXS profiles.) From the absolute scattering intensity, the volume fraction of rods was estimated to be 0.003%, which is sufficiently dilute to ignore rod-rod interactions and below a value where the rods affect the viscoelastic properties of the solutions. (Due to the large atomic number of gold, the nanorods dominate the scattering intensity in the SAXS range even at such dilute volume fractions.) At CPyCl concentrations of 600 mM, SAXS patterns showed an intensity increase in low q, which indicated aggregation of

the rods, and at 800 mM and above, the SAXS patterns revealed macroscopic alignment of the rods, indicating the WLMs formed a nematic phase, consistent with other studies of high-concentration CPyCl/NaSal solutions.⁴⁶ Studies of the nanoparticle dynamics were restricted to isotropic WLM solutions below these concentrations. In addition, from measurements of the densities of the solutions' constituents we found the relation between CPyCl concentration c and micelle volume fraction ϕ to be $\phi = 0.00052 \times (c/mM)$.

C. Rheometry

Measurements of the frequency-dependent complex shear modulus, $G^*(\omega) = G'(\omega) + iG''(\omega)$, were performed using a stress-controlled rheometer (Anton Paar Physica MCR 301) in a cone-plate geometry with a Peltier temperature-control system. The strain amplitude was kept at or below 1%, which was found to be well within the linear regime of stress response.

D. XPCS

XPCS experiments were performed at Sector 8-ID of the Advanced Photon Source. Solutions were contained in glass capillaries with diameter 1.5 mm for transmission scattering. A partially coherent 11 keV x-ray beam of size $20\times20~\mu\text{m}^2$ was incident on the sample. The scattering intensity was recorded at 100 frames per second with a direct-illuminated CCD area detector (LBL-ANL Fast CCD)⁴⁷ with $30\times30~\mu\text{m}^2$ pixel size. The sample-to-detector distance was set at 4.91 m to cover scattering wave vectors q from 0.03 to 0.3 nm⁻¹. Under these conditions, the Siegert factor was 0.103, as measured using a static sample (aerogel). However, above $q \approx 0.11~\text{nm}^{-1}$, the scattering was too weak for reliable determination of the intensity autocorrelation function $g_2(q,t)$, hence we restricted analysis to smaller wave vectors.

III. Results

A. WLM Solution Rheology

We focused on the regime of semidilute WLM solutions with CPyCl concentration in the range 50 < c < 500 mM that form isotropic, entangled solutions. At fixed c, the viscosity of CPyCl/NaSal solutions displays two maxima as a function of NaSal concentration c_s . ^{42, 46, 48} The first maximum is thought to be due to a transition from linear to branched micelles, while the second maximum has been associated with a transition to a nematic phase. ⁴⁶ In the solutions under study, we varied c to tune the entanglement mesh size, and we varied c_s along with c so that the viscosity was always near the first maximum. To maintain this condition, we followed the relation between c and c_s at the first viscosity maximum identified by Rehage and Hoffmann: $\log(c_s/\text{mM}) = 0.23 + 0.8\log(c/\text{mM})$. Additional rheometry measurements on solutions at fixed c and varying c_s confirmed that this relation is valid over the full range, 50 < c < 500 mM.

Figure 1 displays the frequency-dependent complex shear modulus, $G^*(\omega) = G'(\omega) + iG''(\omega)$, of a solution with c = 300 mM (and $c_s = 168$ mM). The modulus follows a form that is characteristic of entangled solutions. At high frequencies, G' > G'', and G' is approximately constant. This plateau is associated with a transient rubbery response due to the mesh of entanglements. At low frequencies, the solutions are fluid, G'' > G', with $G'' \sim \omega$ and with zero-shear-rate viscosity $\eta_0 = \lim_{\omega \to 0} G''(\omega)/\omega$.

The solid lines in the figure display the results of a fit using an empirical Cole-Davidson form⁴⁹ to capture entanglement relaxation, plus a viscous response that accounts for local (Rouse and breathing) motions and becomes appreciable at high frequency,⁵⁰

$$G^*(\omega) = \frac{G_{\infty}}{(1 - i/\omega \tau)^{\alpha}} + i\omega \eta_{\infty}$$
 (2)

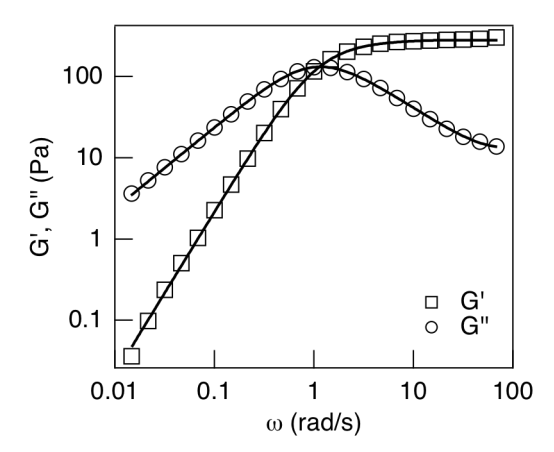


Figure 1. Frequency dependent storage (squares) and loss (circles) moduli of a wormlike micelle solution with CPyCl concentration c = 300 mM and NaSal concentration $c_s = 168$ mM. The solid lines display the results of fits using an empirical Cole-Davidson form plus a viscous contribution to account for short-time-scale dissipation, as described in the text.

where τ is the characteristic relaxation time of the entanglement mesh, G_{∞} is the plateau modulus, the exponent α characterizes the shape of the response, and η_{∞} is the high-frequency viscosity, which falls in the range 0.02-0.1 Pa·s, depending on CPyCl concentration. Equation (2) describes accurately the form of $G^*(\omega)$ over the full range of CPyCl concentrations studied. When α is close to 1, which is the case for the CPyCl/NaSal solutions under study, the Cole-Davidson form approximates the Fourier transform of a stretched exponential response function,

$$G(t) = G_{\infty} e^{-(t/\tau)^{\beta}}, \tag{3}$$

where the exponents α and β are related approximately through $\beta = 0.683\alpha + 0.316$. In the limit $\alpha = 1$, the Cole-Davidson form reduces to that of a Maxwell model (*i.e.*, an exponential stress relaxation, $\beta = 1$, in time domain). The values of β obtained from the results for α from fits to $G^*(\omega)$ at various CPyCl concentrations are shown in Figure 2(a). The exponents are slightly less than one, indicating slight broadening of the relaxation compared to a Maxwell fluid

at frequencies above the peak in G''. According to the model by Cates and coworkers, ⁵²⁻⁵⁴ stress relaxation of WLM solutions displays Maxwell behavior when the average micelle scission time τ_{break} is much less than the reptation time τ_{rep} , in which case the entanglement relaxation time is the geometric mean, $\tau_{er} = \sqrt{\tau_{rep}\tau_{break}}$. In CPyCl/NaSal solutions, the stress relaxation is highly stretched at low c_s , indicating reptation-dominated behavior and crosses over to Maxwell behavior at salt concentrations slightly above the first viscosity maximum, ⁴⁸ suggesting that $\tau_{rep} \gtrsim \tau_{break}$ near the first viscosity maximum, which is the condition in our experiments. ⁴²

Figure 2(b) displays the results for G_{∞} , which describes the transient elastic response of the entangled solutions, at T=25 °C as a function of CPyCl concentration. Similar to other entangled WLM solutions, $^{46}G_{\infty}\sim c^{1.75}$. (Application of scaling theories of polymer physics to WLM solutions predicts slightly stronger concentration dependence, $G_{\infty}\sim c^{2.25}$.) In analogy with rubber elasticity, the characteristic mesh size \mathcal{E} for the entangled micelles, shown in Figure 2(c), can be obtained from G_{∞} through $\mathcal{E}=(k_bT/G_{\infty})^{1/3}$. Figure 2(d) displays the zero-shear-rate viscosity, $\eta_0=\lim_{\omega\to 0}G''(\omega)/\omega$, which characterizes the long-time flow behavior of the solutions. As the dashed line in Figure 2(d) indicates, $\eta_0\sim c^{1.0}$. This dependence on surfactant concentration differs strongly from the theoretically expected relation $\eta_0\sim c^{3.5,46}$ however, such strong deviations from theory are commonly observed in the viscosity of entangled WLM solutions and have been attributed either to the existence of micelle branching 55 or to a concentration-dependent average micelle length that differs from expectations.

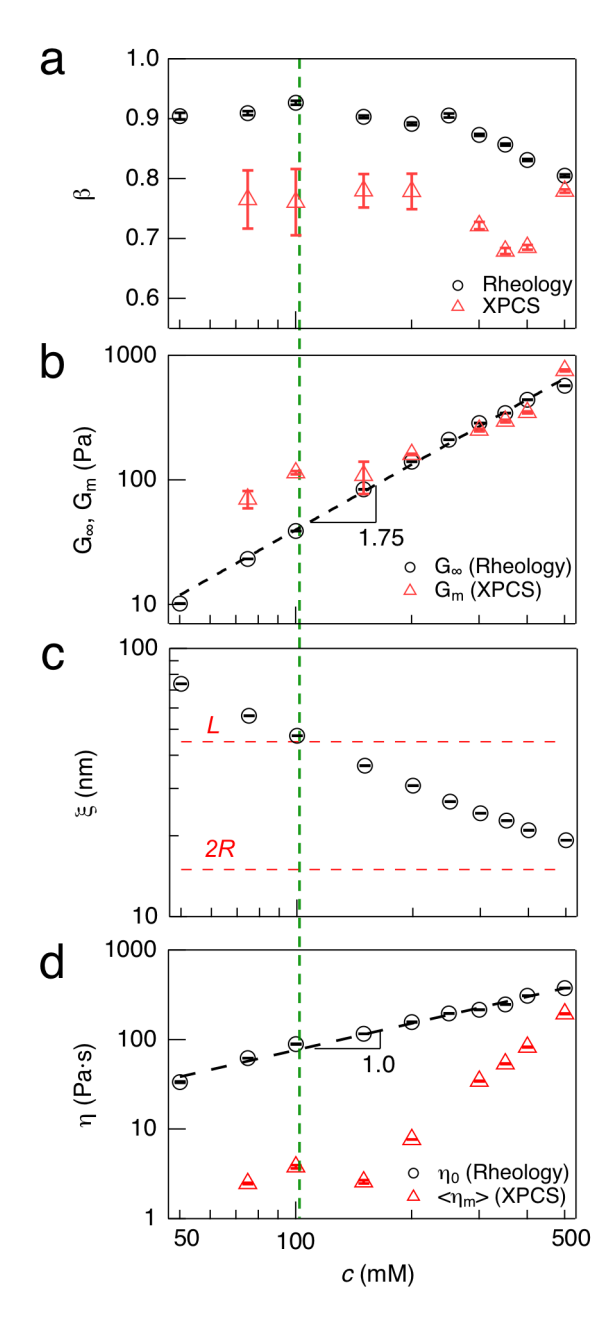


Figure 2. Parameters characterizing solution rheology (circles) and nanorod dynamics (triangles) as a function of CPyCl concentration c. (a) stretching exponent β extracted from fits to the shear modulus and from fits to the XPCS intensity autocorrelation function, (b) plateau modulus G_{∞} determined from rheology and G_m inferred from the short-time localization of the nanorods, (c) entanglement mesh size ξ obtained from G_{∞} , and (d) macroscopic zero-shear-rate viscosity η_0 and microscopic viscosity $<\eta_m>$ obtained from the nanorod diffusivity. The green dashed line denotes the CPyCl concentration at which the mesh size equals the nanorod length.

B. Nanorod Dynamics

In order to gain a microscopic perspective on the structural dynamics in the WLM solutions, we investigated the dynamical behavior of dilute suspensions of nanorods using XPCS. Figure 3 displays the XPCS intensity autocorrelation function $g_2(q,t)$ measured at several wave vectors q on a nanorod dispersion in a WLM solution with c = 300 mM (and $c_s = 168$ mM). In principle, the correlation function reflects both translational and rotational dynamics of the nanorods. However, rotational motion makes appreciable contributions to $g_2(q,t)$ only at large wavevectors, qL > 5, 56 and over the wavevector range in which $g_2(q,t)$ is determined, 0.03 < q < 0.11 nm⁻¹ (1.45 < qL < 5), the correlation function is dictated almost exclusively by translational motion. The solid lines in Figure 3 show the results of fits to $g_2(q,t)$ using a stretched exponential form,

$$g_2(q,t) = 1 + A[\exp[-2(t/\tau)^{\beta}]].$$
 (4)

Such stretched exponential line shapes describe the autocorrelation functions at all wave vectors and CPyCl concentrations. The results for the stretching exponent β are included in Figure 2(a) as a function of CPyCl concentration.

For dilute, noninteracting particles undergoing translational motion in a homogeneous environment, $g_2(q,t)$ is related to the mean-squared displacement, $\langle \Delta r^2(t) \rangle$ through the relation⁵⁷

$$g_2(q,t) = 1 + b \exp[-\langle \Delta r^2(t) \rangle q^2/3]$$
 (5)

where b is the Siegert factor. Hence, one interpretation for the stretched exponential shape of $g_2(q,t)$ is that it implies subdiffusive motion of the rods, $\langle \Delta r^2(t) \rangle \sim t^{\beta}$ and $\beta < 1$. Indeed, subdiffusive nanoparticle motion has been observed in polymer solutions, including in XPCS measurements on spherical particles in entangled solutions. However, we can discount this interpretation for the nanorods in WLM solutions. Another signature of subdiffusive motion is a

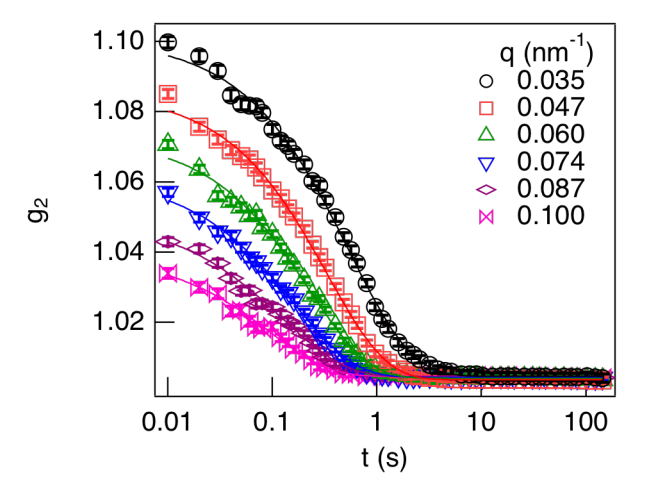


Figure 3. XPCS intensity autocorrelation function $g_2(q,t)$ characterizing the dynamics of gold nanorods in a CPyCl/NaSal 300/168 mM wormlike micelle solution at various wave vectors. The solid lines are the results of fits using a stretched exponential function to the autocorrelation functions.

power-law dependence of the correlation time on wavevector, $\tau \sim q^{-2/\beta}$. In contrast, the correlation times obtained from fits using Eq. (4) follow a significantly weaker q dependence that is consistent with simple diffusion $\tau \sim q^{-2}$, as illustrated in Figure 4(a), which shows the inverse of the mean correlation time, $<\tau^{-1}$, determined through $<\tau > = \tau\Gamma(1/\beta)/\beta$, where Γ is the gamma function. From the observed wavevector dependence, $<\tau^{-1} \sim q^2$, which we see at all surfactant concentrations, we conclude that the nanorods in the WLM solutions undergo simple diffusion and that the stretched-exponential form of $g_2(q,t)$ hence results from spatial heterogeneity in the diffusivity. From the signal-to-noise in $g_2(q,t)$ and the accuracy of the fits over the measurement wavevectors, we estimate that this diffusive motion extends to at least root-mean-squared displacements of 70 nm. That is, this diffusion extends over length scales from r_{loc} to at least several times the entanglement mesh size \mathcal{E} . This behavior contrasts with that

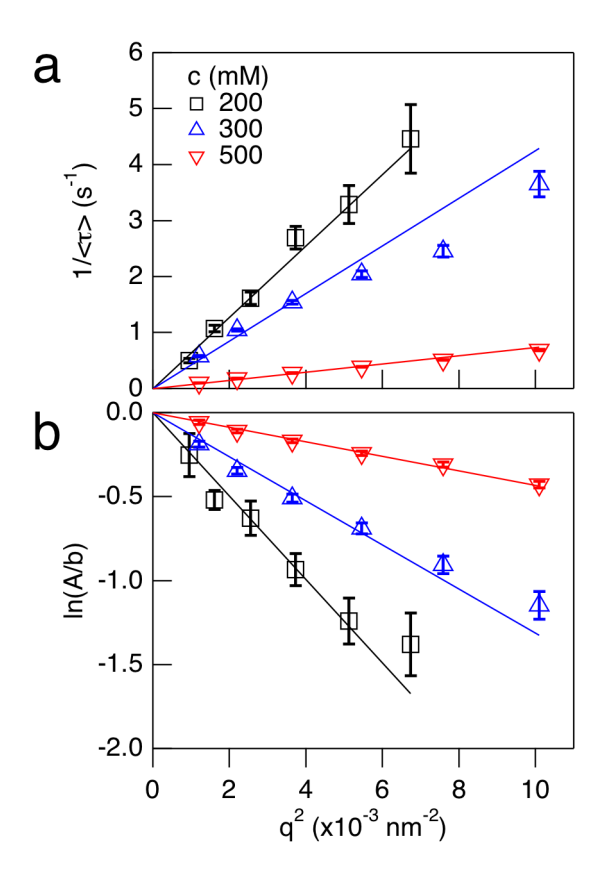


Figure 4. Results characterizing the nanorod dynamics obtained from the XPCS intensity autocorrelation function $g_2(q,t)$ with varying CPyCl concentration c: (a) inverse correlation time $1/\langle \tau \rangle$ and (b) logarithm of the short-time plateau value normalized by the Siegert factor, $\ln(A/b)$, as functions of wave vector squared. In both cases, the solid lines show the results of linear fits.

observed with spherical nanoparticles in entangled polymer solutions, where pronounced subdiffusive motion is observed over similar distances.^{10, 35}

From the fit results shown in Figure 4(a) one can obtain a mean microscopic drag viscosity $\langle \eta_m \rangle$ that the WLM solutions impose on the rods through the relation $\langle \eta_m \rangle = k_b T q^2 \langle \tau \rangle / \zeta$, where ζ is the geometric translational drag coefficient of a rod. Because the measurements average over an isotropic ensemble of rod orientations, we take ζ to be the average of the coefficients parallel ($\zeta_{||}$) and perpendicular (ζ_{\perp}) to the rod axis, $\zeta = (\zeta_{||} + 2\zeta_{\perp})/3 = 294$ nm, where $\zeta_{||} \approx 2\pi L/[\ln(L/2R) - 0.20] = 300$ nm and $\zeta_{\perp} \approx 4\pi L/[\ln(L/2R) + 0.84] = 291$ nm. ⁵⁸ The

resulting values of $\langle \eta_m \rangle$ are shown in Figure 2(d) along with the macroscopic viscosities η_0 as a function of CPyCl concentration. The two viscosities are in approximate agreement at the highest concentration, but they diverge from one another with decreasing concentration, signaling a decoupling of the nanorod diffusivity from the macroscopic solution rheology and hence a breakdown of the Stokes-Einstein relation.

A second feature of the nanorod dynamics is captured in the XPCS measurements by the short-time plateau values of $g_2(q,t)$, which fall below the Siegert factor b and have a strong dependence on q, as illustrated in Figure 3. These plateau values are captured in Eq. (4) by the parameter A, which is plotted in Figure 4(b) normalized by the Siegert factor b. The observation that A is less than b implies the nanorods undergo fast localized motion, creating a partial decay of $g_2(q,t)$ at inaccessibly short times. Specifically, from Eq. (5), one has $A/b = \exp(-r_{loc}^2q^2/3)$ where r_{loc}^2 is the mean squared displacement of the nanorods at short times. Depending on CPyCl concentration, 11 nm $< r_{loc} < 36$ nm. For particles in a Maxwell-like viscoelastic fluid, one can relate r_{loc}^2 to the high-frequency shear modulus by considering, for example, the short-time limit of Eq. (1) to find $r_{loc}^2 = 6k_BT/\zeta G_m$, where G_m is the microscopic transient elasticity. Hence,

$$ln(A/b) = -\frac{2k_bT}{\zeta G_m} q^2 \tag{6}$$

The solid lines in Figure 4(b) show the results of fits using this form. The resulting values of G_m are shown in Figure 2(b) along with the macroscopic high-frequency shear modulus G_∞ as a function of CPyCl concentration. The two quantities agree closely over nearly the full range of surfactant concentrations, but separate below approximately c = 150 mM. The onset of this decoupling occurs near the concentration at which the entanglement mesh size \mathcal{E} becomes larger than the rod length L.

In summary, taking into account both the short-time plateau value and the terminal decay of $g_2(q,t)$, the XPCS measurements provide the following characterization of the nanorod dynamics in the WLM solutions. At short times (t < 0.01 s), which are inaccessible to the measurements, the rods experience a limited range of mobility during which their motion is presumably dictated by Rouse dynamics and other local degrees of freedom of the micelles that control the short-time stress relaxation of the entangled solution. The length scale of this mobility is restricted by caging within the entanglement mesh provided $L > \xi$, such that $<\Delta r^2(t)>$ reaches a temporary plateau at a value r_{loc}^2 that is consistent with expectations based on the solution rheology. On longer times, the rods escape this caging and undergo free diffusion, but they do so on a time scale that is faster than that set by relaxation of the entanglement mesh, hence their diffusivity is larger (effective viscosity is smaller) than that expected from macroscopic rheology.

C. Temperature Dependence of Rheology and Nanorod Dynamics

Further insight into the coupling of the nanorod dynamics to the entanglement mesh and its relaxation comes from comparing the temperature dependence of the nanorod diffusivity with that of the macroscopic viscosity. Figure 5 displays the frequency-dependent shear modulus of the WLM solution with c = 200 mM (and $c_s = 118$ mM) at several temperatures over the range 19 °C < T < 40 °C. Below 19 °C, the rheology undergoes an abrupt change, which we associate with a structural transformation in the micelles induced by a change in miscibility of the CPyCl at low temperature. Above this change, the form of $G^*(\omega)$ is essentially temperature-independent such that the modulus at different temperatures can be superimposed by scaling the angular frequency with a temperature-dependent shift factor a_T with respect to the data at 40 °C, as

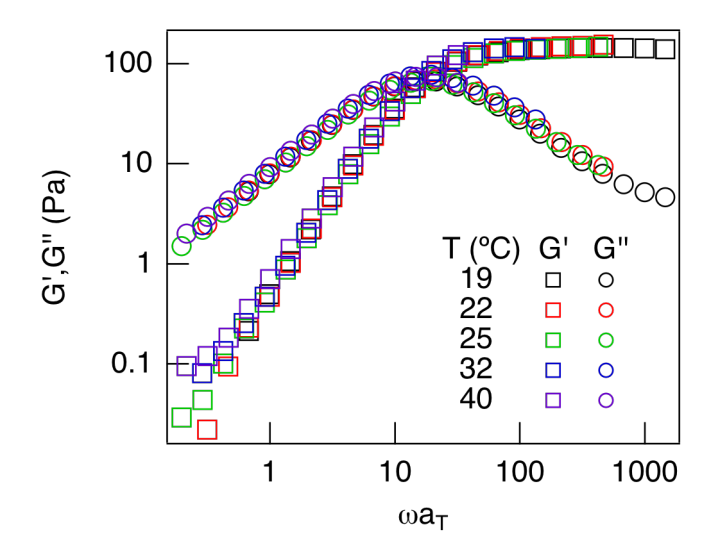


Figure 5. Storage (squares) and loss (circles) moduli of a CPyCl/NaSal solution with c = 200 mM and NaSal concentration $c_s = 118$ mM measured at different temperatures as a function of angular frequency ω scaled with temperature-dependent shift factor a_T .

illustrated in Figure 5. This time-temperature superimposition works equally well for all surfactant concentrations studied. Figure 6(a) shows a_T along with the macroscopic and microscopic viscosities normalized by their respective values at 40 °C for c = 200 mM. Figure 6(b) shows the same quantities for c = 500 mM. Also plotted in the figures is the viscosity of water η_w normalized to its value at 40 °C.⁶⁰ At both high and low surfactant concentration, a_T and η_0 track one another, as expected, and show a strong temperature dependence that results primarily from exponential increases in τ_{break} and in the average micelle length with decreasing temperature that lead to slower entanglement relaxation.⁶¹ At c = 500 mM, $<\eta_m>$ follows a temperature dependence that is nearly as strong as that of η_0 , indicating that the nanorod diffusivity in the concentrated solution is influenced significantly by entanglement relaxation. In contrast, at c = 200 mM, $<\eta_m>$ displays a weaker temperature dependence that is only slightly

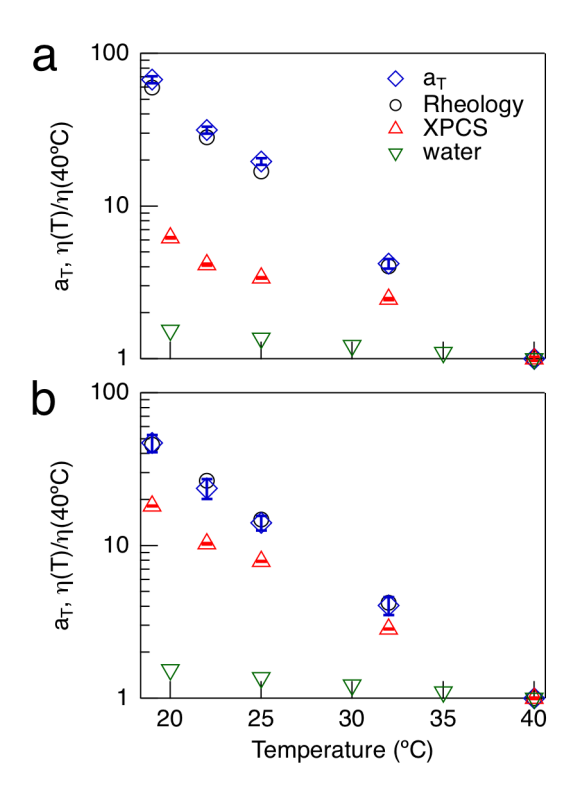


Figure 6. Parameters characterizing WLM solution rheology and nanoparticle dynamics normalized by their values at to their values at 40° C for (a) CPyCl/NaSal (200/118 mM) and (b) CPyCl/NaSal (500/245 mM). Included are the shift factors a_T obtained from scaling the shear moduli, the viscosities obtained from rheology and from the nanorod diffusivity XPCS, and the viscosity of water obtained from Ref. 59.

stronger than that of the solvent viscosity, η_w . Thus, at the lower concentration where $<\eta_m><<\eta_0$, the nanorod mobility is less sensitive to factors that affect entanglement relaxation.

IV. Discussion

A. Review of Recent Theory

The comparison between the rheological parameters obtained via rheometry and those inferred from the nanorod dynamics in Figures 2(b) and 2(d) reveals how the nanoscale structural dynamics that control rod mobility deviate from those dictating macroscopic stress relaxation

when the dimensions of the rods are comparable to the entanglement mesh size. Recent theories of nanoparticle motion in entangled polymers that explain such deviations have taken different approaches to describe the coupling of the size-dependent polymer dynamics to particle dynamics. Addressing the problem of a nanoparticle in an entangled polymer melt, Brochard-Wyart and de Gennes developed a scaling theory for the particle's terminal diffusivity based on the idea that the particle mobility decouples from the macroscopic viscosity when the particle size d is smaller than the tube diameter, which is approximately equivalent to the entanglement mesh size \mathcal{E}^{27} . When $d < \mathcal{E}$, the motion instead becomes dependent on the local relaxation of chain segments of size comparable to the particle. A consequence of this prediction is a sharp discontinuity in diffusivity as the particle size and the entanglement mesh size cross, $d = \mathcal{E}$. Brochard-Wyart and de Gennes further considered both spherical particles and needle-like colloids, for which they predicted a regime of anisotropic diffusion when the needle diameter was smaller than the tube diameter but the length was larger. \mathcal{E}^{27}

Recently, Cai *et al.* expanded these scaling ideas to address not only the terminal diffusivity but also shorter-time particle dynamics and to describe nanoparticle mobility in entangled solutions.²⁸ They also developed a model of "hopping" diffusion relevant for the regime in which the particle size is slightly larger than the mesh size.²⁹ In this model, activated motion in which the particle overcomes the free energy barrier imposed by the cage of chains in the local entanglement mesh provides a channel for diffusion in parallel with relaxation of the mesh. This process removes the discontinuity in diffusivity at $d = \mathcal{E}$ in the Brochard-Wyart and de Gennes model and leads to particle mobilities in excess of macroscopic expectations for particle sizes up to several times that of the entanglement mesh size.

In an alternative approach to understanding nanoparticle motion in entangled polymer melts, Yamamoto and Schweizer developed a microscopic force-level theory based on a self-consistent generalized Langevin equation.^{30, 33} For small particles, the theory reproduces the scaling results of Brochard-Wyart and de Gennes, but it also captures the gradual nature of the coupling between a particle and the full entanglement network constraints as the particle size increases past $d = \mathcal{E}$. As a result, the theory predicts significantly enhanced diffusion for particles somewhat larger than the mesh size, with Stokes-Einstein behavior recovered only at $d \approx 10\mathcal{E}$. Such enhanced diffusivity over macroscopic expectations by particles in the range $\mathcal{E} < d < 10\mathcal{E}$ has been confirmed in experiments and simulations.^{8, 35} In the context of the theory, Dell and Schweizer further considered activated hopping but concluded that it contributed negligibly to particle mobility except for a narrow range of conditions.³¹

B. Possible Role of Anisotropic Diffusion in Nanorod Dynamics

As mentioned above, Brochard-Wyart and de Gennes predicted highly anisotropic mobility of a needle-shaped colloid in an entangled polymer when the colloid size is in the range $2R < \xi < L$.²⁷ In this regime, the colloid experiences only a local nanoviscosity when diffusing parallel to its axis, but diffusion perpendicular to the axis requires full relaxation of the entangled chains. As shown in Figure 2(c), the range of ξ covered in the experiments matches this condition. Therefore, within the Brochard-Wyart and de Gennes model we can potentially interpret the deviations between $<\eta_m>$ and η_0 with the enhanced diffusivity of the rods in the direction parallel to their axes. This idea is supported by the weak temperature dependence of low-concentration $<\eta_m>$ in Figure 5(a), since the nanoviscosity is determined by the relaxation of chain segments up to size 2R through Rouse dynamics and hence is independent of the factors

causing the strong temperature dependence of η_0 , specifically τ_{break} and micelle length. However, other aspects of this model of anisotropic diffusion appear at odds with the observed mobility of the nanorods and lead us to doubt its relevance. First, if the diffusivity is indeed set by the relaxation of chain segments of size comparable to 2R, then scaling theory predicts $<\eta_m>\sim c^{1.5},^{28}$ which is in strong contrast with the trend in Figure 2(d). Second, the model of anisotropic diffusion, as developed by Brochard-Wyart and de Gennes, predicts a discontinuity in diffusivity as \mathcal{E} crosses 2R. Since $<\eta_m>$ approaches η_0 smoothly at the highest concentrations in Figure 2(d) where \mathcal{E} approaches 2R, the results appear to be inconsistent with such a discontinuity.

Another concern regarding the suitability of an anisotropic diffusion model to explain the rod mobility is the similarity between G_{∞} and G_m above c=100 mM, which implies that the rods remain elastically coupled to the entanglement mesh as long as \mathcal{E} is smaller than the rod length L. This agreement suggests that the rod length rather than the diameter is the relevant dimension in dictating the rods' entrainment in the mesh. This conclusion is also supported by the recent work of Cai *et al.*²⁹ and of Yamamoto and Schweizer³³ described above that, through different theoretical approaches, predict that nanoparticle diffusivity converges to the value expected macroscopically from the Stokes-Einstein relation only when the particle size is several times larger than the entanglement mesh size. As the results in Figure 2 show, $<\eta_m>$ approaches η_0 as L approaches $3\mathcal{E}$, and hence the nanorod dynamics are consistent with the conclusions of Cai *et al.* and of Yamamoto and Schweizer provided the rod length is the relevant scale to compare with the entanglement mesh size. Thus, while significantly anisotropic diffusion might play a role in dictating mobility of nanorods of higher aspect ratio in entangled polymers, ¹¹ for the nanorods in this study with a modest aspect ratio near 3, it appears not to be important.

C. Possible Role of Hopping Diffusion in Nanorod Dynamics

As mentioned above, both the recent theories of Cai *et al.*²⁹ and of Yamamoto and Schweizer³³ provide predictions for nanoparticle diffusivity in entangled polymers when the particle size is somewhat larger than the entanglement mesh. Here we focus on that of Cai *et al.*²⁹, whose work includes predictions for nanoparticles in entangled solutions that we can compare with the results for the diffusivity of the nanorods in the WLM solutions. (This focus does not discount the possibility that the predictions of Yamamoto and Schweizer³³ properly recast might not successfully describe the results.) As described above, Cai *et al.* have proposed a mechanism for particle motion through the entanglement mesh based on "hopping" diffusion that can contribute to particle mobility as long as the particle size is not too much larger than the mesh.²⁹ Based on this idea and scaling arguments from polymer physics, they have derived an expression for particle diffusivity as function of polymer concentration $D(\phi)$. (See Eq. (F.4) in Ref. ²⁹.) Modifying the dependence on ϕ in their expression to account for the scaling behavior we have obtained empirically for the CPyCl/NaSal solutions (specifically, $G_{\infty} \sim \phi^{1.75}$ and $\eta_0 \sim \phi^{1.0}$) and taking the characteristic size of a nanorod to be its length L, we find:

$$D(\phi) = \frac{kT}{\zeta_m N_o^2(1)} \phi^{0.58} exp \left[-\frac{L}{a_o(1)} \phi^{0.58} \right] + B\phi^{-1}$$
 (7)

where B is a constant described below, ζ_m is the "monomeric friction coefficient", and $a_e(1)$ and $N_e(1)$ are the tube diameter and the number of Kuhn lengths in an entanglement segment, respectively, that one would have in the melt. (The theory neglects numerical factors of order unity in the prefactor and in the exponential of the first term.) This diffusivity can be related to the effective viscosity felt by a nanorod, and hence this prediction can be compared directly to the XPCS results, through $D(\phi) = kT/\xi < \eta_m >$. The first term in Eq. (7) is the contribution from

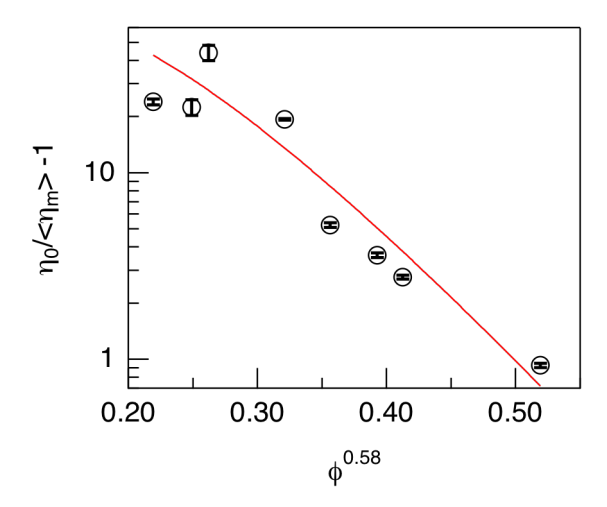


Figure 7. The ratio of macroscopic viscosity η_0 to the viscosity obtained from the nanorod diffusivity $\langle \eta_m \rangle$ minus one versus $\phi^{0.58}$, where ϕ is the micelle volume fraction. The solid line shows the result of a fit using the form predicted by a model of "hopping" diffusion (Eq. 8), as described in the text.

"hopping". The second is the contribution from entanglement relaxation and is simply the expected diffusivity based on the macroscopic viscosity through the Stokes-Einstein relation, $B\phi^{I} = kT/\xi\eta_{-}$. From the results for η_{-} in Figure 2(d), we obtain $B = 9.5 \times 10^{-18}$ m²/s, where we convert from CPyCl concentration c to micelle concentration ϕ using the measured relation, $\phi = 0.00052(c/\text{mM})$.

To highlight the enhanced mobility of the rods over macroscopic expectations, we rewrite Eq. (7) in terms of the ratio of the macroscopic and microscopic viscosities,

$$\frac{\eta_0}{\langle \eta_m \rangle} - 1 = \frac{kT}{B\zeta_m N_e^2(1)} \phi^{1.58} exp \left[-\frac{L}{a_e(1)} \phi^{0.58} \right]. \tag{8}$$

Figure 7 displays the results for $\eta_{-}/<\eta_{m}>$ - 1 plotted against $\phi^{0.58}$, and the solid line in the figure shows the result of a fit to the data using Eq. (8), which gives the fit parameters $\zeta_{m}N_{e}^{2}(1)=1.51(\pm0.6)\times10^{-9}~\mathrm{N\cdot s/m}$ and $a_{e}(1)=2.2\pm0.2~\mathrm{nm}$. As the figure indicates, the agreement between the fit and the data is good, supporting the applicability of the "hopping" diffusion model in

explaining the enhanced mobility of the nanorods in the entangled WLM solutions. The values obtained for the fit parameters reinforce this support. Specifically, the result for $a_e(1)$ is the same order of magnitude as the micelle diameter, $a_m \approx 4$ nm,⁶² as one would expect for the tube diameter if one could create a "melt" of wormlike micelles. Also, if one approximates the monomeric friction factor as $\zeta_m = 3\pi a_m \eta_w$, then for $a_m = 4$ nm and the aqueous solvent of viscosity $\eta_w = 10^{-3}$ Pa·s one obtains $\zeta_m = 3.8 \times 10^{-11}$ N·s/m. Combined with the fit result for $\zeta_m N_e^2(1)$ above, this approximation gives $N_e(1) = 6$, which is again a reasonable order-of-magnitude estimate. Indeed, given that the expression derived by Cai *et al.* for $D(\phi)$ relies on the scaling behavior of solutions of flexible polymers and neglects numerical factors of order unity, we find the agreement in Figure 7 between the predicted diffusivity and that of the nanorods in the WLM solutions to be remarkable.

V. Conclusions

In conclusion, the results presented in this paper on the mobility of nanorods in entangled WLM solutions illustrate the effectiveness of XPCS in interrogating the nanometer-scale motion of nanoparticles within complex-fluid environments. Figure 8 depicts schematically the relationship between the XPCS correlation function measured on the nanorods in the WLM solutions and the corresponding nanorod mean squared displacement. A key aspect of the XPCS results is the q-dependent apparent amplitude of $g_2(q,t)$ that is smaller than the Siegert factor (A(q) < b), implying two temporally separated regimes of nanorod motion. In the first regime, which occurs on time scales that are too small for the measurement to capture, the nanorod motion is restricted to a localization length set by the transient elasticity of the entangled micelles in agreement with a generalized Stokes-Einstein relation, provided the entanglement

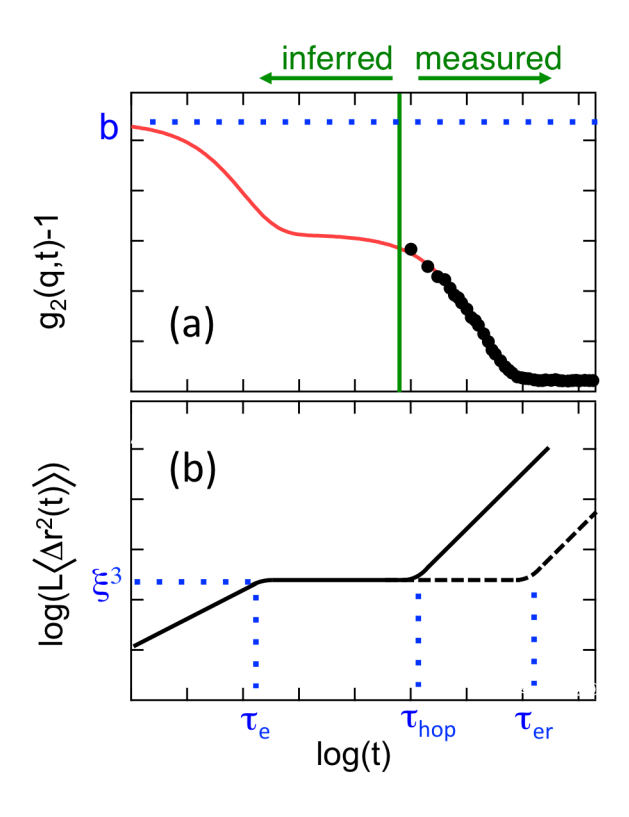


Figure 8. Schematic representations of (a) the XPCS intensity correlation function and (b) the corresponding nanorod mean-squared displacement over an extended time range. The data in (a) are the results from Figure 3 for $g_2(q,t)$ at q = 0.074 nm⁻¹. The solid line in (a) is the result of a fit to the data at large t using a stretched exponential lineshape with a second, partial decay at shorter t incorporated to account for the difference between the amplitude of $g_2(q,t)$ in the measured range and the Siegert factor b. As depicted in (b), the observed terminal decay in $g_2(q,t)$ corresponds to diffusion of the nanorods, which occurs at a rate set by the hopping diffusion time τ_{hop} . In the absence of hopping diffusion, the diffusivity would be smaller and would be set by the entanglement relaxation time τ_{er} . The first partial decay of $g_2(q,t)$ corresponds to motion of the nanorods localized to a range $\langle \Delta r^2(t) \rangle \approx \xi^3/L$. We infer that these short-time dynamics are dictated by their coupling of the nanorods to Rouse dynamics and that extend to the relaxation time of an entanglement strand τ_e , as discussed in Reference 29.

mesh size is smaller than the nanorod length. As mentioned above, these short-time dynamics are presumably dictated by Rouse dynamics that lead to subdiffusive motion at short times.^{28, 30,}

The second regime, which controls the terminal decay of $g_2(q,t)$, is characterized by a long-

time diffusivity of the nanorods that exceeds the diffusivity expected from the Stokes-Einstein relation by an amount that agrees remarkably with the predictions of "hopping" nanoparticle diffusion in entangled polymer solutions. This agreement is perhaps surprising given the microscopic differences between WLM solutions and polymer solutions. Further studies on other types of nanoparticle/entangled-polymer systems would help clarify whether this agreement is fortuitous or whether the theory indeed has broad applicability.

Interesting future XPCS experiments would extend such measurements to smaller t to capture the initial, partial decay of $g_2(q,t)$ and hence to characterize the nanorod dynamics at times and distances before the effects of entanglement confinement develop, when the motion should be affected by micelle segments below the entanglement length.^{28, 33} While such measurements would be challenging for XPCS today, they should become more feasible following anticipated improvements in the technique, for example through the advent of high-frame-rate x-ray area detectors⁶³ and through the proposed upgrades of the Advanced Photon Source and other synchrotron sources to diffraction-limited storage rings whose greatly improved x-ray brightness promises to revolutionize the dynamic range of XPCS.⁶⁴

Another interesting future direction would be XPCS experiments involving nanorods with larger aspect ratio in entangled polymer and WLM solutions. Large aspect ratio should lead to clearer evidence of anisotropic diffusivity expected when $2R < \xi < L$. Further, such measurements that access dynamics at high wave vector (qL > 5) should probe the rotational diffusion of the rods⁵⁶ and thus explore the coupling of rotational and translational mobility.³⁸ In particular, since free rotation of a rod involves motion over a length scale of L/2, the degree to which rotational diffusion is constrained by entanglements should vary with ξ as long as $\xi < L/2$. Finally, nanoparticles with the requisite surface properties have been shown to act as end points

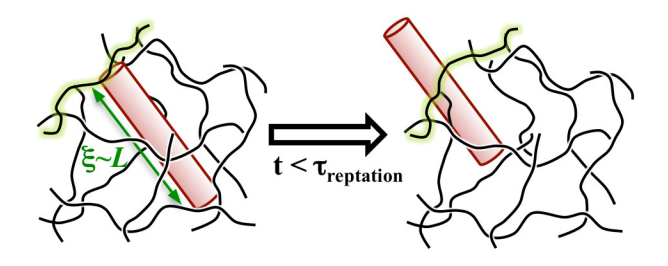
for wormlike micelles and thereby to serve as junctions in the formation of micellar networks.^{65,}

While focused potentially in different scientific questions than we have addressed here, XPCS experiments probing the nanoparticle dynamics in such materials could provide further insight into the nanoscale structural dynamics of these interesting composite materials.

Acknowledgements

This research used resources of the Advanced Photon Source and the Center for Nanoscale Materials, U.S. Department of Energy (DOE) Office of Science User Facilities operated for the DOE Office of Science by Argonne National Laboratory under Contract No. DE-AC02-06CH11357. JL acknowledges the support from Argonne's LDRD program. AGI acknowledges a scholarship from CAPES/PDSE (BEX 3193/14-4). RLL thanks the Argonne National Laboratory X-ray Science Division Visiting Scientist Program for support. The authors also acknowledge the Brazilian funding agency CNPq (Grant 477467/2010-5) and the National Science Foundation (NSF DMR-1207117 and DMR-1610875).

TOC Figure:



References

- 1. Winey, K. I.; Vaia, R. A. Polymer Nanocomposites. MRS Bull. 2007, 32 (04), 314-322.
- 2. Mackay, M. E.; Tuteja, A.; Duxbury, P. M.; Hawker, C. J.; Van Horn, B.; Guan, Z.; Chen, G.; Krishnan, R. S. General Strategies for Nanoparticle Dispersion. *Science* **2006**, 311 (5768), 1740-1743.
- 3. Balazs, A. C.; Emrick, T.; Russell, T. P. Nanoparticle Polymer Composites: Where Two Small Worlds Meet. *Science* **2006**, 314 (5802), 1107-1110.
- 4. Kim, D.; Srivastava, S.; Narayanan, S.; Archer, L. A. Polymer nanocomposites: polymer and particle dynamics. *Soft Matter* **2012**, 8 (42), 10813-10818.
- 5. Ensign, L. M.; Schneider, C.; Suk, J. S.; Cone, R.; Hanes, J. Mucus Penetrating Nanoparticles: Biophysical Tool and Method of Drug and Gene Delivery. *Adv. Mater.* **2012**, 24 (28), 3887-3894.
- 6. Suk, J. S.; Xu, Q.; Kim, N.; Hanes, J.; Ensign, L. M. PEGylation as a strategy for improving nanoparticle-based drug and gene delivery. *Adv. Drug Deliv. Rev.* **2016,** 99, Part A, 28-51.
- 7. Grabowski, C. A.; Mukhopadhyay, A. Size Effect of Nanoparticle Diffusion in a Polymer Melt. *Macromolecules* **2014**, 47 (20), 7238-7242.
- 8. Chapman, C. D.; Lee, K.; Henze, D.; Smith, D. E.; Robertson-Anderson, R. M. Onset of Non-Continuum Effects in Microrheology of Entangled Polymer Solutions. *Macromolecules* **2014**, 47 (3), 1181-1186.
- 9. Guo, H.; Bourret, G.; Corbierre, M. K.; Rucareanu, S.; Lennox, R. B.; Laaziri, K.; Piche, L.; Sutton, M.; Harden, J. L.; Leheny, R. L. Nanoparticle Motion within Glassy Polymer Melts. *Phys. Rev. Lett.* **2009**, 102 (7), 075702.
- 10. Guo, H.; Bourret, G.; Lennox, R. B.; Sutton, M.; Harden, J. L.; Leheny, R. L. Entanglement-Controlled Subdiffusion of Nanoparticles within Concentrated Polymer Solutions. *Phys. Rev. Lett.* **2012**, 109 (5), 055901.
- 11. Choi, J.; Cargnello, M.; Murray, C. B.; Clarke, N.; Winey, K. I.; Composto, R. J. Fast Nanorod Diffusion through Entangled Polymer Melts. *ACS Macro Lett.* **2015**, 4 (9), 952-956.
- 12. Babaye Khorasani, F.; Poling-Skutvik, R.; Krishnamoorti, R.; Conrad, J. C. Mobility of Nanoparticles in Semidilute Polyelectrolyte Solutions. *Macromolecules* **2014**, 47 (15), 5328-5333.
- 13. Tuteja, A.; Mackay, M. E.; Narayanan, S.; Asokan, S.; Wong, M. S. Breakdown of the continuum Stokes-Einstein relation for nanoparticle diffusion. *Nano Lett.* **2007**, 7 (5), 1276-1281.
- 14. Alam, S.; Mukhopadhyay, A. Translational and Rotational Diffusions of Nanorods within Semidilute and Entangled Polymer Solutions. *Macromolecules* **2014**, 47 (19), 6919-6924.
- 15. Holyst, R.; Bielejewska, A.; Szymanski, J.; Wilk, A.; Patkowski, A.; Gapinski, J.; Zywocinski, A.; Kalwarczyk, T.; Kalwarczyk, E.; Tabaka, M.; Ziebacz, N.; Wieczorek, S. A. Scaling form of viscosity at all length-scales in poly(ethylene glycol) solutions studied by fluorescence correlation spectroscopy and capillary electrophoresis. *Phys. Chem. Chem. Phys.* **2009**, 11 (40), 9025-9032.
- 16. Jee, A.-Y.; Curtis-Fisk, J. L.; Granick, S. Nanoparticle Diffusion in Methycellulose Thermoreversible Association Polymer. *Macromolecules* **2014**, 47 (16), 5793-5797.

- 17. Omari, R. A.; Aneese, A. M.; Grabowski, C. A.; Mukhopadhyay, A. Diffusion of Nanoparticles in Semidilute and Entangled Polymer Solutions. *J. Phys. Chem. B* **2009**, 113 (25), 8449-8452.
- 18. Ziebacz, N.; Wieczorek, S. A.; Kalwarczyk, T.; Fialkowski, M.; Holyst, R. Crossover regime for the diffusion of nanoparticles in polyethylene glycol solutions: influence of the depletion layer. *Soft Matter* **2011**, 7 (16), 7181-7186.
- 19. Kohli, I.; Mukhopadhyay, A. Diffusion of Nanoparticles in Semidilute Polymer Solutions: Effect of Different Length Scales. *Macromolecules* **2012**, 45 (15), 6143-6149.
- 20. Szymański, J.; Patkowski, A.; Wilk, A.; Garstecki, P.; Holyst, R. Diffusion and Viscosity in a Crowded Environment: from Nano- to Macroscale. *J. Phys. Chem. B* **2006**, 110 (51), 25593-25597.
- 21. Poling-Skutvik, R.; Mongcopa, K. I. S.; Faraone, A.; Narayanan, S.; Conrad, J. C.; Krishnamoorti, R. Structure and Dynamics of Interacting Nanoparticles in Semidilute Polymer Solutions. *Macromolecules* **2016**, 49 (17), 6568-6577.
- 22. de Kort, D. W.; Rombouts, W. H.; Hoeben, F. J. M.; Janssen, H. M.; Van As, H.; van Duynhoven, J. P. M. Scaling Behavior of Dendritic Nanoparticle Mobility in Semidilute Polymer Solutions. *Macromolecules* **2015**, 48 (20), 7585-7591.
- 23. Mangal, R.; Srivastava, S.; Narayanan, S.; Archer, L. A. Size-Dependent Particle Dynamics in Entangled Polymer Nanocomposites. *Langmuir* **2016**, 32 (2), 596-603.
- 24. Hoshino, T.; Murakami, D.; Tanaka, Y.; Takata, M.; Jinnai, H.; Takahara, A. Dynamical crossover between hyperdiffusion and subdiffusion of polymer-grafted nanoparticles in a polymer matrix. *Phys. Rev. E* **2013**, 88 (3), 032602.
- 25. Ruta, B.; Czakkel, O.; Chushkin, Y.; Pignon, F.; Nervo, R.; Zontone, F.; Rinaudo, M. Silica nanoparticles as tracers of the gelation dynamics of a natural biopolymer physical gel. *Soft Matter* **2014**, 10 (25), 4547-4554.
- 26. Poling-Skutvik, R.; Krishnamoorti, R.; Conrad, J. C. Size-Dependent Dynamics of Nanoparticles in Unentangled Polyelectrolyte Solutions. *ACS Macro Lett.* **2015**, 4 (10), 1169-1173.
- 27. Brochard Wyart, F.; de Gennes, P. G. Viscosity at small scales in polymer melts. *Eur. Phys. J. E* **2000**, 1 (1), 93-97.
- 28. Cai, L. H.; Panyukov, S.; Rubinstein, M. Mobility of Nonsticky Nanoparticles in Polymer Liquids. *Macromolecules* **2011**, 44 (19), 7853-7863.
- 29. Cai, L.-H.; Panyukov, S.; Rubinstein, M. Hopping Diffusion of Nanoparticles in Polymer Matrices. *Macromolecules* **2015**, 48 (3), 847-862.
- 30. Yamamoto, U.; Schweizer, K. S. Theory of nanoparticle diffusion in unentangled and entangled polymer melts. *J. Chem. Phys.* **2011,** 135 (22), 224902.
- 31. Dell, Z. E.; Schweizer, K. S. Theory of Localization and Activated Hopping of Nanoparticles in Cross-Linked Networks and Entangled Polymer Melts. *Macromolecules* **2014**, 47 (1), 405-414.
- 32. Dong, Y.; Feng, X.; Zhao, N.; Hou, Z. Diffusion of nanoparticles in semidilute polymer solutions: A mode-coupling theory study. *J. Chem. Phys.* **2015**, 143 (2), 024903.
- 33. Yamamoto, U.; Schweizer, K. S. Microscopic Theory of the Long-Time Diffusivity and Intermediate-Time Anomalous Transport of a Nanoparticle in Polymer Melts. *Macromolecules* **2015**, 48 (1), 152-163.
- 34. Egorov, S. A. Anomalous nanoparticle diffusion in polymer solutions and melts: A mode-coupling theory study. *J. Chem. Phys.* **2011**, 134 (8), 084903.

- 35. Kalathi, J. T.; Yamamoto, U.; Schweizer, K. S.; Grest, G. S.; Kumar, S. K. Nanoparticle Diffusion in Polymer Nanocomposites. *Phys. Rev. Lett.* **2014**, 112 (10), 108301.
- 36. Ganesan, V.; Pryamitsyn, V.; Surve, M.; Narayanan, B. Noncontinuum effects in nanoparticle dynamics in polymers. *J. Chem. Phys.* **2006**, 124 (22), 221102.
- 37. Pryamitsyn, V.; Ganesan, V. Noncontinuum effects on the mobility of nanoparticles in unentangled polymer solutions. *J. Polym. Sci. Part B: Polym. Phys.* **2016**.
- 38. Kim, M. J.; Cho, H. W.; Kim, J.; Kim, H.; Sung, B. J. Translational and rotational diffusion of a single nanorod in unentangled polymer melts. *Phys. Rev. E* **2015**, 92 (4), 042601.
- 39. Liu, J.; Cao, D.; Zhang, L. Molecular Dynamics Study on Nanoparticle Diffusion in Polymer Melts: A Test of the Stokes–Einstein Law. *J. Phys. Chem. C* **2008**, 112 (17), 6653-6661.
- 40. Squires, T. M.; Mason, T. G. Fluid Mechanics of Microrheology. *Annu. Rev. Fluid Mech.* **2010,** 42, 413-438.
- 41. Xu, J.; Viasnoff, V.; Wirtz, D. Compliance of actin filament networks measured by particle-tracking microrheology and diffusing wave spectroscopy. *Rheol. Acta* **1998**, 37 (4), 387-398.
- 42. Rehage, H.; Hoffmann, H. Rheological Properties of Viscoelastic Surfactant Systems. *J. Phys. Chem.* **1988**, 92 (16), 4712-4719.
- 43. Leheny, R. L. XPCS: nanoscale motion and rheology. *Curr. Opin. Colloid Interface Sci.* **2012,** 17, 3-12.
- 44. Leheny, R. L.; Rogers, M. C.; Chen, K.; Narayanan, S.; Harden, J. L. Rheo-XPCS. *Curr. Opin. Colloid Interface Sci.* **2015**, 20 (4), 261-271.
- 45. Ye, X.; Jin, L.; Caglayan, H.; Chen, J.; Xing, G.; Zheng, C.; Doan-Nguyen, V.; Kang, Y.; Engheta, N.; Kagan, C. R.; Murray, C. B. Improved Size-Tunable Synthesis of Monodisperse Gold Nanorods through the Use of Aromatic Additives. *ACS Nano* **2012**, 6 (3), 2804-2817.
- 46. Berret, J. F., Rheology of Wormlike Micelles: Equilibrium Properties and Shear Banding Transitions. In *Molecular Gels: Materials with Self-Assembled Fibrillar Networks*, Weiss, R. G.; Terech, P., Eds. Springer Netherlands: Dordrecht, 2006; pp 667-720.
- 47. Doering, D.; Andresen, N.; Contarato, D.; Denes, P.; Joseph, J. M.; McVittie, P.; Walder, J. P.; Weizeorick, J.; Zheng, B. High speed, direct detection 1k Frame-Store CCD sensor for synchrotron radiation. Proceedings of Nuclear Science Symposium and Medical Imaging Conference (NSS/MIC), 2011 IEEE pp 1840-1845.
- 48. Rehage, H.; Hoffmann, H. Viscoelastic surfactant solutions: model systems for rheological research. *Mol. Phys.* **1991,** 74 (5), 933-973.
- 49. Davidson, D. W.; Cole, R. H. Dielectric Relaxation in Glycerol, Propylene Glycol, and n Propanol. *J. Chem. Phys.* **1951**, 19 (12), 1484-1490.
- 50. Berret, J. F.; Appell, J.; Porte, G. Linear rheology of entangled wormlike micelles. *Langmuir* **1993**, 9 (11), 2851-2854.
- 51. Lindsey, C. P.; Patterson, G. D. Detailed comparison of the Williams–Watts and Cole–Davidson functions. *J. Chem. Phys.* **1980**, 73 (7), 3348-3357.
- 52. Cates, M. E. Reptation of living polymers: dynamics of entangled polymers in the presence of reversible chain-scission reactions. *Macromolecules* **1987**, 20 (9), 2289-2296.
- 53. Cates, M. E. Dynamics of living polymers and flexible surfactant micelles: scaling laws for dilution. *J. Phys. France* **1988**, 49, 1593-1600.
- 54. Granek, R.; Cates, M. E. Stress relaxation in living polymers: Results from a Poisson renewal model. *J. Chem. Phys.* **1992**, 96 (6), 4758-4767.

- 55. Lequeux, F.; Candau, S. J., Dynamical Properties of Wormllike Micelles Deviations from the Classical Picture. In *Structure and Flow in Surfactant Solutions*, Herb, C. A.; Prudhomme, R. K., Eds. 1994; Vol. 578, pp 51-62.
- 56. Dhont, J. K. G., *An Introduction to Dynamics of Colloids*. Elsevier Science: Amsterdam, 1996.
- 57. Berne, B. J.; Pecora, R., Dynamic Light Scattering with Applications to Chemistry, Biology, and Physics. Dover: Mineola, 2000.
- 58. Tirado, M. M.; de la Torre, J. G. Translational friction coefficients of rigid, symmetric top macromolecules. Application to circular cylinders. *J. Chem. Phys.* **1979**, 71 (6), 2581-2587.
- 59. Bandyopadhyay, R.; Liang, D.; Yardimci, H.; Sessoms, D. A.; Borthwick, M. A.; Mochrie, S. G. J.; Harden, J. L.; Leheny, R. L. Evolution of particle-scale dynamics in an aging clay suspension. *Phys. Rev. Lett.* **2004**, 93 (22), 228302.
- 60. Kestin, J.; Sokolov, M.; Wakeham, W. A. Viscosity of liquid water in the range -8 °C to 150 °C. *J. Phys. Chem. Ref. Data* **1978**, 7 (3), 941-948.
- 61. Cates, M. E.; Candau, S. J. Statics and dynamics of worm-like surfactant micelles. *J. Phys. Condens. Matter* **1990**, 2 (33), 6869.
- 62. Porte, G.; Marignan, P.; Bassereau, P.; May, R. Shape transformations of the aggregates in dilute surfactant solutions: a small angle neutron scattering study. *J. Phys. France* **1988**, 49, 511-519.
- 63. Zhang, Q.; Dufresne, E. M.; Grybos, P.; Kmon, P.; Maj, P.; Narayanan, S.; Deptuch, G. W.; Szczygiel, R.; Sandy, A. Submillisecond X-ray photon correlation spectroscopy from a pixel array detector with fast dual gating and no readout dead-time. *J. Synchrotron Rad.* **2016**, 23 (3), 679-684.
- 64. Shpyrko, O. X-ray photon correlation spectroscopy. *J. Synchrotron Rad.* **2014,** 21 (5), 1057-1064.
- 65. Helgeson, M. E.; Hodgdon, T. K.; Kaler, E. W.; Wagner, N. J.; Vethamuthu, M.; Ananthapadmanabhan, K. P. Formation and Rheology of Viscoelastic "Double Networks" in Wormlike Micelle—Nanoparticle Mixtures. *Langmuir* **2010**, 26 (11), 8049-8060.
- 66. Helgeson, M. E.; Wagner, N. J. Colloidal interactions mediated by end-adsorbing polymer-like micelles. *J. Chem. Phys.* **2011**, 135 (8), 084901.
- 67. Ilavsky, J.; Jemian, P. R. Irena: tool suite for modeling and analysis of small-angle scattering. J. Appl. Cryst. **2009**, 42 (2), 347-353.